

1 **Suv420 enrichment at the centromere limits Aurora B localization and function**

2

3

4 Conor P Herlihy^{1, 2}, Sabine Hahn¹, Nicole M Hermance¹, Elizabeth A Crowley¹, and
5 Amity L Manning^{1*}

6

7 ¹ Department of Biology and Biotechnology, Worcester Polytechnic Institute, Worcester,
8 MA, 01609 USA

9 ² Current location is Department of Genetics, Harvard Medical School, Boston, MA,
10 02115 USA

11

12 *Corresponding author:

13 Amity L Manning

14 Email: almanning@wpi.edu

15 tel: 508-831-4961

16

17

18 Running title: H4K20me3-dependent regulation of Aurora B

19

20 Key words:

21 **Centromere**

22 **Mitosis**

23 **CIN**

24 **Abstract**

25 Centromere structure and function are defined by the epigenetic modification of histones
26 at centromeric and pericentromeric chromatin. The constitutive heterochromatin found at
27 pericentromeric regions is highly enriched for H3K9me3 and H4K20me3. While mis-
28 expression of the methyltransferase enzymes, Suv39 and Suv420, that regulate these
29 marks are common in disease, the consequences of such changes are not well
30 understood. Our data show that increased centromere localization of Suv39 and Suv420
31 suppress centromere transcription and compromise localization of the mitotic kinase
32 Aurora B: decreasing microtubule dynamics and compromising chromosome alignment
33 and segregation. We find that inhibition of Suv420 methyltransferase activity partially
34 restores Aurora B localization to centromeres and that restoration of the Aurora B-
35 containing CPC to the centromere is sufficient to suppress mitotic errors that result when
36 Suv420/H4K20me3 is enriched at centromeres. Consistent with a role for Suv39 and
37 Suv420 in negatively regulating Aurora B, high expression of these enzymes
38 corresponds with increased sensitivity to Aurora kinase inhibition in cancer cells
39 suggesting that increased H3K9 and H4K20 methylation may be an underappreciated
40 source of chromosome missegregation in cancer.

41

42 **Introduction**

43 Mitotic chromosome segregation is regulated, in part, through the composition and
44 function of kinetochores, which are protein complexes that link spindle microtubules to
45 chromatin (Thomas et al., 2017, Hinshaw and Harrison, 2018). Kinetochores are, in turn,
46 assembled upon specialized domains of chromatin known as centromeres. Centromeric
47 chromatin is comprised of highly repetitive DNA sequences and is defined epigenetically
48 by the presence of the centromere-specific histone 3 variant CENP-A (Hinshaw and
49 Harrison, 2018, De Rop et al., 2012, Sharma et al., 2019, Ohzeki et al., 2019, Guse et

50 al., 2011, Carroll and Straight, 2006). Flanking the CENP-A containing centromeric
51 chromatin are less ordered repeat sequences that make up the pericentromere. A
52 defining characteristic of pericentromeric chromatin is its enrichment for repressive
53 epigenetic marks, including di- and tri- methylation of lysine 9 on histone H3 and lysine
54 20 on histone H4 (H3K9me_{2/3} and H4K20me_{2/3}, respectively), that are strikingly absent
55 from the adjacent centromere (Fioriniello et al., 2020, Sullivan and Karpen, 2004). While
56 CENP-A chromatin is demonstrated to be a critical epigenetic marker upon which the
57 kinetochore is built (De Rop et al., 2012, Barnhart et al., 2011), the function of the
58 epigenetic marks at pericentromeric heterochromatin (PCH) domains remain less clear.

59
60 While many studies have implicated changes in heterochromatin in the regulation of
61 genome stability and cancer progression, most focus on the consequences of decreased
62 H3K9me₃ and H4K20me₃ heterochromatin marks (reviewed in Janssen et al., 2018).
63 Nevertheless, both increased expression of the methyltransferases responsible for
64 placing these repressive marks and decreased expression of demethylases that remove
65 these marks, have been described in various cancer contexts (Janssen et al., 2018,
66 Black et al., 2012, Zhou et al., 2019, Yokoyama et al., 2013). Functional studies in
67 cancer cells indicate that increased levels of H3K9me₃ and H4K20me₃ contribute to
68 increased motility and metastatic potential (Zhou et al., 2019, Yokoyama et al., 2013)
69 and can limit therapeutic response (Cuellar et al., 2017, Guler et al., 2017).

70
71 Studies exploiting a human artificial chromosome (HAC) system have shown that
72 expansion of heterochromatin via direct tethering of Suv39 to the centromere is sufficient
73 to compromise segregation fidelity of the HAC (Ohzeki et al., 2012, Martins et al., 2016).
74 Consistent with these observations, recent work has revealed that expression of Suv39
75 and Suv420, the methyltransferases responsible for H3K9me_{2/3} and H4K20me_{2/3}

76 respectively, correlate with levels of aneuploidy across 10,000+ cancer samples from the
77 Cancer Genome Atlas Project (Taylor et al., 2018). Mitotic segregation errors underlie
78 the generation of aneuploidy and together these data suggest that misregulation of
79 Suv39 and Suv420, and the epigenetic marks they regulate, may be functionally linked
80 to the generation of aneuploidy in cancer.

81
82 Key to accurate chromosome segregation is the localization and function of the mitotic
83 kinase Aurora B (Lampson et al., 2004, Liang et al., 2020, Gregan et al., 2011, Krenn
84 and Musacchio, 2015). Aurora B, together with INCENP, Survivin, and Borealin, form the
85 chromosomal passenger complex (CPC). Distributed along chromosome arms at mitotic
86 entry, the CPC re-localizes first to the centromere and kinetochore and later during
87 anaphase to the central spindle (Hindriksen et al., 2017). Concentration of the CPC at
88 the centromere and kinetochore is believed to be crucial for its function in mitotic error
89 correction as it places Aurora B in close proximity to its substrates on kinetochores
90 (Welburn et al., 2010). Aurora B de-stabilizes microtubules by phosphorylating several
91 key regulators of kinetochore-microtubule attachments to promote the removal of
92 merotelic attachments (Cheeseman et al., 2006, Welburn et al., 2010, DeLuca et al.,
93 2011, Cimini et al., 2006, DeLuca et al., 2006). The formation of merotelic attachments
94 during early stages of mitosis are stochastic and loss or functional inactivation of Aurora
95 B kinase activity precludes their correction and corrupts mitotic fidelity (Abe et al., 2016,
96 Broad et al., 2020, Hauf et al., 2003, Huang et al., 2018).

97

98 An intricate signaling network involving Haspin-dependent phosphorylation of H3T3 and
99 Bub1-dependent phosphorylation of H2AT120 controls localization of the CPC to the
100 inner centromere. These pathways represent two parallel modes of CPC regulation such
101 that abrogation of either one results in dispersion of the CPC over chromatin and a

102 reduction, but not loss, of CPC at the centromere (Hindriksen et al., 2017, Krenn and
103 Musacchio, 2015, Carretero et al., 2013, Dai et al., 2006, Meppelink et al., 2015, Wang
104 et al., 2010). It remains unclear whether other epigenetic marks at the centromere or
105 pericentromere similarly impact the regulation of CPC localization and function.

106

107 **Results**

108 **High expression of Suv39 and Suv420 methyltransferases is prevalent in cancer**

109 Expression data from the TCGA indicate that Suv39 and Suv420 are highly expressed in
110 cancer contexts, with Suv39 isoforms h1 and h2 and Suv420 isoform h2 exhibiting
111 increased average expression compared to corresponding normal tissue in eleven of
112 fourteen cancer subtypes for which paired tumor and normal data is available. (Figure
113 1A). These enzymes function to regulate constitutive heterochromatin at
114 pericentromeres and in normal cells H3K9me3 and H4K20me3 are enriched near
115 centromeres. In a panel of high Suv420-expressing breast cancer cell lines H4K20me3
116 is not dispersed uniformly throughout the genome and instead remains enriched near
117 centromeres (Supplemental Figure 1), raising the possibility that Suv420 misexpression
118 may preferentially compromise pericentromere or centromere function and perturb
119 mitotic chromosome segregation. Indeed, recent work describes that high expression of
120 Suv39 or Suv420 positively correlates with pan cancer analyses of increased aneuploidy
121 (Taylor et al., 2018). This relationship is not an artifact of high Suv39 or Suv420
122 expression in a single cancer type that also happens to be highly aneuploid but instead
123 persists when samples are sorted by cancer subtype. We find that high expression of at
124 least one Suv39 or Suv420 isoform demonstrate a significant positive correlation with
125 aneuploidy in twelve out of twenty cancer contexts represented in the TCGA database
126 (Figure 1B, Supplemental Table 1). Consistent with a correlation with aneuploidy, which
127 is known to correspond with tumor aggressiveness and poor patient outcome (Pfau and

128 Amon, 2012, Weaver et al., 2007, Davoli et al., 2013, Liu et al., 2016), high expression
129 of a Suv39h1/h2 or Suv420h1/h2 isoform corresponds with a significant decrease in
130 disease free survival in four out of twenty cancer subtypes represented in the GEO, EGA
131 and TCGA databases (Supplemental Table 2) (Nagy et al., 2018, Györfy et al., 2010).

132

133 **Depletion of the H3K9me3 demethylase KDM4A compromises mitotic fidelity**

134 To define the consequences of increased H3K9 and H4K20 methylation on mitotic
135 chromosome segregation we used multiple independent approaches to increase the
136 methylated state of H3K9 or H4K20 globally or specifically at the centromere in hTERT-
137 immortalized human retinal pigment epithelial (RPE-1) cells. RPE-1 cells are diploid and
138 genomically stable, exhibiting fewer than one segregation error every 100 cell divisions
139 (Thompson and Compton, 2008). To enhance H3K9 methylation and monitor the impact
140 on mitosis we first utilized siRNA to deplete KDM4A, a demethylase responsible for
141 removing di- and tri-methyl marks from H3K9 (Supplemental Figure 2A) (Berry and
142 Janknecht, 2013). As expected, depletion of KDM4A led to a small but measurable
143 increase in the global level of H3K9 methylation (Supplemental Figure 2D & E). Using
144 time-lapse and fixed cell imaging approaches, we demonstrate that depletion of KDM4A
145 compromises mitotic progression. RPE-1 cells expressing RFP-tagged histone 2B (RFP-
146 H2B) to label chromatin were transfected with non-targeting control (siControl) or
147 KDM4A-targeting siRNA (siKDM4A) for 36 hours and then monitored by live cell
148 fluorescence imaging (Figure 2A). Images were captured every 5 minutes and mitotic
149 cells were tracked to determine the dynamics of chromosome alignment and the timing
150 of anaphase onset. Cells lacking KDM4A exhibit a minor delay in metaphase
151 chromosome alignment and anaphase onset (27.37 +/- 0.40 minutes vs. 34.67 +/- 1.33
152 minutes, $p = 0.007$; Figure 2A). Consistent with live cell imaging, immunofluorescence
153 analysis of KDM4A-depleted cells reveal an enrichment in cells where single

154 chromosomes remain near spindle poles when metaphase alignment of the majority of
155 chromosomes has already been achieved (Figure 2B). Although live cell imaging reveals
156 that full metaphase alignment is eventually achieved prior to anaphase onset, nearly
157 25% of KDM4A-depleted anaphase cells exhibit lagging chromosomes (Figure 2C).
158 Similar results were seen when KDM4A mRNA was targeted for depletion with any one
159 of four independent siRNA sequences (Supplemental Figure 2B, Supplemental Table 3).

160

161 **Centromere tethering of the histone methyltransferase Suv39 or Suv420 corrupt**
162 **mitotic fidelity**

163 As H3K9 methylation is not exclusive to the pericentromere, increased H3K9 methylation
164 that follows KDM4A depletion is not restricted to centromere or pericentromere
165 heterochromatin (Supplemental Figure 2D & E) (Berry and Janknecht, 2013). Therefore,
166 to test if changes in centromere-specific H3K9 methylation levels are sufficient to cause
167 mitotic errors, we engineered RPE-1 cells to inducibly express a GFP-tagged Suv39h1
168 protein fused to the DNA binding domain of the centromere localized protein CENP-B
169 (cen-Suv39-GFP, Supplemental Figure 2C-E). The DNA binding domain of CENP-B
170 binds to a discrete sequence at the centromere (Pluta et al., 1992), targeting the cen-
171 Suv39-GFP fusion protein to centromeres where it promotes increased H3K9
172 methylation (Supplemental Figure 2D & E). Comparable to depletion of KDM4A,
173 immunofluorescence imaging of cells following induced expression of cen-Suv39-GFP
174 revealed an increase in metaphase cells with alignment defects and anaphase cells with
175 lagging chromosomes that are not present in the absence of doxycycline-induced
176 expression of the transgene (i.e. Mock vs. Induced: Supplemental Figure 3B, Figure 3A).

177

178 H3K9 methylation promotes recruitment and binding of heterochromatin protein 1 (HP1).
179 HP1 in turn serves as a platform to recruit a number of factors to heterochromatin,

180 including the H4K20 methyltransferase Suv420 (Janssen et al., 2018, Hahn et al., 2013,
181 Schotta et al., 2004). Thus, establishment of H3K9me3 by Suv39 is indirectly implicated
182 in deposition of H4K20me3. Consistent with this relationship, we find that centromere
183 targeting of Suv39 (the H3K9me2/3 methyltransferase) enhances H4K20me3 levels at
184 the centromere (Figure 3B). To delineate the roles of H3K9 and H4K20 centromere
185 methylation in the regulation of mitotic progression we next expressed a GFP-tagged
186 Suv420h2 protein fused to the DNA binding domain of centromere protein CENP-B (cen-
187 Suv420-GFP). Cen-Suv420-GFP localizes to centromeres and is sufficient to promote a
188 marked enrichment of H4K20me3 at centromeres without altering H4K20me3 levels
189 along chromosome arms (Figure. 3B, Supplemental Figure 3C). As seen with KDM4A
190 depletion and cen-Suv39-GFP expression, induced expression of cen-Suv420-GFP
191 leads to metaphase alignment defects (Supplemental Figure 3B) and anaphase
192 segregation errors (Figure 3A), suggesting that increased H4K20me3 at centromeres is
193 sufficient to corrupt kinetochore regulation. Chromosomes that lag during anaphase can
194 be excluded from the main nucleus when the nuclear envelope reforms, resulting in the
195 formation of a separate micronucleus. Consistent with the presence of chromosome
196 segregation defects, cells expressing cen-Suv39-GFP or cen-Suv420-GFP also exhibit
197 an increase in the number of interphase cells within the population that have
198 centromere-positive micronuclei (Figure 3C).

199

200 **Centromere enrichment of Suv420 compromises mitotic error correction** 201 **mechanisms**

202 Formation of syntelic and merotelic microtubule attachments, where both kinetochores of
203 a chromosome pair are bound by microtubules from the same spindle pole, occur
204 stochastically during mitosis. Error correction mechanisms to destabilize such mal-
205 attachments persist throughout prometaphase and metaphase (Cimini et al., 2003).

206 Delays in chromosome alignment to the metaphase plate, and the presence of lagging
207 chromosomes during anaphase, can result from persistent merotelic attachments and
208 may indicate that the number of merotelic attachments formed in mitosis overwhelm the
209 error correction machinery (Cimini et al., 2003). Imbalances in error corrective
210 mechanisms that result in merotelic attachments and segregation errors arise due to
211 either an increased burden in the number of merotelic attachments formed, or from an
212 underlying defect in the error correction machinery. To determine if cells with altered
213 centromere methylation are predisposed to forming merotelic attachments or instead are
214 deficient in correcting these mal-attachments, KDM4A-depleted cells or those induced to
215 express either cen-Suv39-GFP or cen-Suv420-GFP were exposed to the Eg5 inhibitor
216 monastrol for 4 hours (Figure 4A). Inhibition of the mitotic kinesin Eg5 causes spindle
217 poles to collapse, resulting in a monopolar spindle structure. These spindles cannot form
218 amphitelic chromosome attachments and instead form syntelic or monotelic
219 attachments. Upon washout of monastrol, a large portion of kinetochore attachments are
220 converted to merotelic attachments (Kapoor et al., 2000, Lampson et al., 2004).
221 Destabilization of mal-attached microtubules is a prerequisite for acquisition of proper
222 kinetochore biorientation and chromosome alignment such that the time needed to
223 achieve complete metaphase alignment following monastrol washout is an indication of
224 error correction efficiency. Immunofluorescence imaging demonstrates that, following
225 monastrol washout, bipolar spindles form and the majority of control cells restore
226 chromosome biorientation and achieve metaphase alignment within 40 minutes. In
227 contrast, though spindle bipolarity is achieved similarly to control cells, KDM4A-depleted,
228 cen-Suv39-GFP expressing and cen-Suv420-GFP expressing cells all exhibit a delayed
229 progression to metaphase, with fewer than half of all cells able to achieve metaphase
230 alignment within the same time frame as control cells (Figure 4A). Together, these data

231 indicate that the mitotic error correction machinery is compromised under conditions
232 where H3K9me3 or H4K20me3 is increased.

233

234 **Centromere localization of the CPC is sensitive to centromere enrichment of**
235 **Suv39 or Suv420**

236 Aurora B is a mitotic kinase that functions as a master regulator of error correction. Loss
237 or functional inactivation of Aurora B kinase activity leads to persistent merotelic
238 attachments and segregation errors (Lampson et al., 2004, Liang et al., 2020, Gregan et
239 al., 2011, Krenn and Musacchio, 2015, Kallio et al., 2002, Hauf et al., 2003, Ditchfield et
240 al., 2003). To determine if changes in Aurora B, localization and/or function underlie
241 observed defects in mitosis following manipulations that increase H3K9me3 and/or
242 H4K20me3, we first performed quantitative immunofluorescence to measure Aurora B
243 and INCENP (a component of the Aurora B-containing CPC complex) recruitment to
244 centromeres following expression of either cen-Suv39-GFP or cen-Suv420-GFP, or
245 depletion of KDM4A. By measuring pixel intensity of Aurora B or INCENP antibody
246 staining across kinetochore pairs stained with anti-centromere antigen (ACA) in
247 metaphase and/or nocodazole-arrested prometaphase cells we identified and assessed
248 Aurora B localization at centromeres and kinetochores. We find that the intensity of both
249 Aurora B and INCENP at mitotic centromeres is significantly reduced following depletion
250 of KDM4A or induced expression of either cen-Suv39-GFP or cen-Suv420-GFP (Figure
251 4, Supplemental Figure 4). Aurora B, Borealin, INCENP, and Survivin are all expressed
252 at similar levels in cells with and without induction of cen-Suv39-GFP or cen-Suv420-
253 GFP, suggesting that decreased staining intensity is not a consequence of changes in
254 CPC expression (Supplemental Figure 4C). Importantly, expression of centromere
255 targeted GFP alone (cen-GFP) or non-targeted Suv420 (Suv420-GFP), conditions that
256 do not enhance centromere enrichment of H4K20me3, do not perturb centromere levels

257 of Aurora B (Figure 4, Supplemental Figures 3 and 4). Instead, reduction in centromere
258 localization of CPC components is sensitive to Suv420 and/or H4K20me3 at
259 centromeres as treatment with A196, a specific small molecule inhibitor of Suv420
260 methyltransferase activity (Bromberg et al., 2017), is sufficient to partially restore Aurora
261 B localization to centromeres and to promote efficient chromosome alignment along the
262 metaphase plate (Figure 5).

263

264 Phosphorylation of Hec1 (at serine 55) by Aurora B de-stabilizes kinetochore
265 microtubule attachments to permit error correction. Consistent with compromised Aurora
266 B localization, we find centromeres in mitotic cells have decreased Hec1
267 phosphorylation, but not overall levels of Hec1, when cen-Suv39-GFP or cen-Suv420-
268 GFP is expressed (Figure 6A & B). These cells also exhibit a corresponding increase in
269 stable microtubules that are resistant to cold-induced depolymerization (Figure 6C). A
270 similar decrease is seen in phosphorylation levels of Aurora B target CENP-A (at serine
271 7) at centromeres (Supplemental Figure 5A & B). However, consistent with other
272 conditions that specifically perturb Aurora B activity at centromere but not along
273 chromosome arms (Wang et al., 2010), no change is seen in the phosphorylation of H3
274 (at serine 10), a substrate of Aurora B on chromosome arms (Supplemental Figure 5C).

275 Aurora B localization to centromeres is influenced by several histone modifications,
276 including phosphorylation of threonine 120 on histone 2A (H2A-T120p) by BUB1 and
277 phosphorylation of threonine 3 on histone 3 (H3-T3p) by Haspin. Each of these histone
278 phosphorylation events is independently sufficient to recruit Aurora B to centromeres
279 (Liang et al., 2020, Broad et al., 2020, Hadders et al., 2020). However, we do not see
280 reduction in either of these histone marks in contexts where H4K20me3 has been
281 directly or indirectly increased (Supplemental Figure 6A & B), suggesting indirect

282 changes in these known regulatory marks cannot explain decreased centromere CPC
283 complex localization.

284 Localization of the CPC is also sensitive to centromere transcription. Centromere
285 transcripts have been shown to bind the CPC and regulate both CPC centromere
286 localization and Aurora B activation (Jambhekar et al., 2014, Blower, 2016, Ideue et al.,
287 2014). To test whether centromere transcription is altered by centromere tethering of
288 Suv39-GFP or Suv420-GFP we measured levels of centromere transcripts in
289 nocodazole-synchronized cells following 24 hours of cen-Suv39-GFP or cen-Suv420-
290 GFP expression. While qPCR analysis shows expression of centromeric α satellite RNA
291 is readily detected during mitosis, levels of each transcript were reduced by roughly half
292 in mitotic cells expressing cen-Suv39-GFP or cen-Suv420-GFP (Supplemental Figure
293 6C). Consistent with the centromere tethering of these constructs, suppression of
294 transcription appears restricted to centromeres as transcripts from non-centromere
295 regions, such as housekeeping genes (GAPDH and actin) and CPC components remain
296 unchanged in these samples (Supplemental Figure 4C). These data suggest that
297 suppression of transcription underlies defects in Aurora B localization when centromere
298 levels of Suv39/H3K9me3 and/or Suv420/H4K20me3 are increased.

299 **Expression level of Suv39 and Suv420 correspond with sensitivity to Aurora** 300 **kinase inhibition in cancer cell lines**

301 Decreased CPC localization and increased rates of chromosome segregation errors may
302 render cells exquisitely sensitive to further inhibition of Aurora kinase activity. To test this
303 possibility, cells with and without induction of cen-Suv39-GFP or cen-Suv420-GFP
304 expression were treated with inhibitors targeting Aurora B Kinase (Barasertib), the
305 related Aurora A kinase (Alisertib), or the mitotic kinase MPS1 and monitored for mitotic

306 fidelity. While control, cen-Suv39-GFP and cen-Suv420-GFP expressing cells were all
307 similarly sensitive to MPS1 inhibition, we find that cells expressing cen-Suv39-GFP or
308 cen-Suv420-GFP are susceptible to increased anaphase lagging chromosomes
309 following short term treatment with low nanomolar concentrations of both Aurora kinase
310 inhibitors, while control cells are not (Figure 7A). We next tested whether mitotic defects
311 in cen-Suv420-GFP expressing cells could be suppressed by concurrently tethering the
312 Aurora B containing CPC to the centromere. Cen-Suv420-GFP expressing cells were
313 monitored for anaphase defects following expression of cen-INCENP-mCherry (Wang et
314 al., 2011). Cells expressing cen-Suv420 exhibit a high rate of lagging chromosomes
315 during anaphase (Figures 3A & 7E). The frequency of these defects was reduced when
316 the cen-INCENP-mCherry construct was expressed simultaneously. Importantly, the
317 level of cen-Suv420-GFP at centromeres was not significantly altered following cen-
318 INCENP-mCherry expression (Figure 7B-D), suggesting this rescue is not the result of a
319 competition between INCENP and Suv420 for centromere binding.

320

321 To explore this relationship more broadly, we utilized the drug sensitivity data described
322 by the Wellcome Sanger Institute (Yang et al., 2013) and RNAseq expression data from
323 the Cancer Cell Line Encyclopedia that includes 1,457 cancer cell lines (Ghandi et al.,
324 2019). Cell lines were sorted based on Suv39 or Suv420 expression level and then drug
325 sensitivity of the top and bottom quartiles compared. We found that cell lines likely to
326 have high H3K9 and/or H4K20 methylation states (due to high expression of Suv39 or
327 Suv420) exhibit increased sensitivity to 5 out of 6 inhibitors that preferentially target
328 Aurora kinase activity (Alisertib, CD532, GSK1070916, Genentech-CPD-10, and
329 ZM447439) (Fig. 7F). This relationship does not reflect a general sensitivity to mitotic
330 poisons as inhibition of the mitotic kinase MPS1 (MPS1IN1, TK3146) do not indicate a
331 similar correlation with expression of these epigenetic regulators.

332

333 **Discussion**

334 Here we demonstrate that Aurora B recruitment to centromeres is sensitive to changes
335 in the epigenetic regulation of pericentromeric heterochromatin. We find that increased
336 methylation of H3K9 and H4K20 corresponds with reduced Aurora B localization to
337 centromeres and reduced phosphorylation of Aurora B substrates. Consistent with
338 studies that directly perturb Aurora B function (Kallio et al., 2002, Hauf et al., 2003,
339 Ditchfield et al., 2003), we show that such changes in centromere levels of the
340 methyltransferases Suv39 or Suv420 are sufficient to stabilize kinetochore microtubule
341 dynamics, limit merotelic error correction, increase lagging chromosomes during
342 anaphase, and promote whole chromosome segregation errors.

343

344 **Suv39 and Suv420 overexpression contribute to increased aneuploidy**

345 Analyses presented here and previously reported by The Meyerson group (Taylor et al.,
346 2018) indicate a moderate but highly significant correlation between degree of
347 aneuploidy and the independent expression levels of Suv39h1, Suv39h2, Suv420h1,
348 and Suv420h2. Consistent with previous reports, our experimental data indicate that
349 these isoforms of Suv39 and Suv420 also share at least partially overlapping roles in
350 heterochromatin regulation and mitotic fidelity (Tsang et al., 2010, O'Carroll et al., 2000).
351 As such, we expect that misexpression of any one of these enzymes (Suv39h1,
352 Suv39h2, Suv420h1, or Suv420h2) could be sufficient to promote segregation errors and
353 that the correlation of an individual enzyme with degree of aneuploidy would therefore be
354 lower than if the function were served by a single enzyme. Though the correlation with
355 aneuploidy for each enzyme is moderate, given the high significance of this relationship,
356 we propose these correlations are consistent with a model whereby high expression
357 levels of a Suv39 or Suv420 isoform are sufficient to promote mitotic defects and

358 contribute to the generation of aneuploidy. Our data does not argue against the
359 possibility that Suv39 or Suv420 function outside regulation of pericentromere
360 heterochromatin may compromise genome stability in cancer. However, our
361 experimental data showing that centromere enrichment of Suv420/H4K20me3 is
362 sufficient to compromise mitotic fidelity, together with sustained pericentromere
363 enrichment of H4K20me3 in cancer cells with high expression of Suv420, suggest that
364 corruption of centromere regulation may be a contributing factor.

365

366 **Short term changes in centromere H3K9me3 and/or H4K20me3 corrupt mitotic**
367 **fidelity without apparent defects in gross centromere structure**

368 Work from other groups has described that a persistent increase in H3K9me3 over many
369 cell cycles limits CENP-A deposition at the centromere on a human artificial
370 chromosome (HAC), thus compromising centromere maintenance (Ohzeki et al., 2012,
371 Martins et al., 2016, Martins et al., 2020). However, while induction of cen-Suv39-GFP or
372 cen-Suv420-GFP for 24h (less than two cell cycles) is sufficient to cause dramatic
373 changes in centromere levels of H3K9me3 and/or H4K20me3, it appears insufficient to
374 compromise centromere formation or maintenance as we detect no change in overall
375 levels of CENPA at the centromere, or in the outer kinetochore protein Hec1
376 (Supplemental Figure 5, Figure 6). Consistent with the sustained localization of critical
377 centromere and outer kinetochore proteins, we find that cells expressing cen-Suv39-
378 GFP or cen-Suv420-GFP remain competent to form stable end-on microtubule
379 attachments that are sufficient to drive chromosome movement and segregation.
380 However, we find that short-term increases in Suv39 and/or Suv420 at centromeres
381 compromised CPC localization and reduced phosphorylation of Aurora B substrates,
382 suggesting that spreading of the respective heterochromatin marks can impact
383 centromere function in two distinct ways: first by subtly moderating regulation of

384 microtubule attachments, and then more crudely by preventing centromere formation
385 and maintenance. As methylation levels likely increase with duration of the experimental
386 perturbation, these distinctions may arise due to experimental differences in the total
387 amount of H3K9/H4K20 methylation achieved at the centromere, or instead reflect a
388 cumulative impact of persistent epigenetic deregulation over several cell cycles remains
389 unclear.

390

391 **Both direct and indirect increases in H4K20me3 levels corrupt mitotic fidelity**

392 In otherwise normal cells, depletion of KDM4A, or overexpression of Suv420 alone
393 promotes aberrant methylation throughout the genome; however changes in H4K20me3
394 at the centromere are moderate (Figure 3 B, (Manning et al., 2014)), suggesting that
395 additional regulatory pathways may function to limit Suv420 enrichment or otherwise
396 restrict H4K20me3 at centromeres. Nevertheless, this regulation of centromere/
397 pericentromere Suv420 localization may not be as tightly controlled in cancer contexts
398 as we find that H4K20me3 remains enriched at centromeres in a panel of breast cancer
399 cell lines that highly express Suv420 (Supplemental Figure 1). Furthermore, our study
400 demonstrates that centromere targeting of Suv420 is sufficient to enhance H4K20me3
401 levels at centromeres without increasing H4K20me3 along chromosome arms. In this
402 way, while we can not rule out that H3K9me3 independently impairs Aurora B
403 localization at centromeres, our data suggest that increased Suv420 and/or H4K20me3,
404 independent of Suv39/H3K9me3, is sufficient to restrict Aurora B localization and
405 compromise mitotic fidelity. Importantly, expression of centromere-targeted GFP, even at
406 levels higher than that of cen-Suv39-GFP or cen-Suv420-GFP, is insufficient to alter
407 centromere H4K20me3 or Aurora B localization (Figures 3B & 4B). Together, these data
408 suggest that Aurora B localization and mitotic fidelity are not generally perturbed by

409 protein tethering to the centromere but are instead specifically sensitive to Suv420
410 and/or H4K20me3 levels.

411

412 Our data indicate that KDM4a depletion may disrupt Aurora B localization without a
413 significant change in centromere H4K20me3 levels (Figure 3). Unlike expression of the
414 cen-targeted constructs whose GFP tag allows us to confirm that each mitotic
415 cell/centromere analyzed has overexpressed the enzyme, we do not have a similar
416 report of KDM4A depletion at the single cell level and can not rule out the possibility that
417 changes in methylation/Aurora B staining at centromeres may be impacted by variability
418 of KDM4A depletion with the cell population. Nevertheless, our rescue experiments
419 showing that inhibition of Suv420 methyltransferase activity (with A196) incompletely
420 restores Aurora B localization (Figure 5) is consistent with Aurora B localization being at
421 least partially independent of H4K20me3 levels.

422

423 HP1 directly binds the Aurora B-containing CPC through INCENP, and in doing so
424 enhances the enzymatic activity of Aurora B (Abe et al., 2016, Kang et al., 2011). In turn,
425 Aurora B-dependent phosphorylation of H3S10 limits HP1 association with H3K9
426 methylation (Fischle et al., 2005, Hirota et al., 2005), such that the interaction between
427 HP1 and Aurora B both positively (through functional regulation) and negatively (through
428 reduction of HP1 recruitment) regulates Aurora B activity at the centromere. Suv420 is
429 similarly recruited to the pericentromere through interactions with HP1 and our data raise
430 the possibility that CPC interaction with HP1 is limited when Suv420 is bound.
431 Consistent with this possibility, we find that centromere-localization of the CPC is
432 disrupted by centromere tethering of Suv420, but not overexpression of non-tethered
433 Suv420. Interestingly, if true, this model would suggest that Suv420's role in regulating
434 CPC localization were in part independent of its methyltransferase activity.

435

436 **Disruption of heterochromatin boundaries impair centromere cohesion,**
437 **transcription, and function.**

438 The constitutive heterochromatin marks H3K9me3 and H4K20me3 are enriched at
439 pericentromeres but normally restricted from the core of the centromere (Sullivan and
440 Karpen, 2004). This dynamic boundary between centromeric and pericentromeric
441 heterochromatin is defined by H3K9 methylation and its disruption impacts transcription
442 of the underlying DNA (Lam et al., 2006). In our experiments, the Suv39 and Suv420
443 fusion constructs target methyltransferase activity to centromeres by exploiting the
444 CENP-B DNA binding domain. This binding domain recognizes a 17bp motif at
445 centromeres to which the constitutive centromere protein CENP-B localizes (Muro et al.,
446 1992). In recruiting Suv39 and Suv420 to this domain H3K9 and H4K20 methylation
447 increases at ACA-stained centromeres indicating that heterochromatin, and potentially
448 heterochromatin-associated proteins, has spread from the pericentromere into the
449 centromere. Consistent with spreading of heterochromatin, we find levels of centromere
450 and pericentromere transcripts are reduced following tethering of Suv39 or Suv420 to
451 mitotic centromeres (Supplemental Figure 6C). In future studies, it will be important to
452 determine if CPC recruitment and centromere function is generally sensitive to increased
453 Suv420 at centromere/pericentromere regions, or specifically sensitive to the spreading
454 of the repressive H4K20me3 mark into the centromere, where it is normally absent.

455

456 Early in mitosis Aurora B is localized along chromosome arms and must be re-localized
457 to centromeres to ensure accurate chromosome segregation. Various regulatory
458 mechanisms for recruitment and retainment of Aurora B to centromeres have been
459 identified including positive regulation by phosphorylation of H3T3 and H2AT120
460 (Yamagishi et al., 2010, Kelly et al., 2010, Wang et al., 2010, Tsukahara et al., 2010).

461 However, our data indicate that neither H3T3 phosphorylation nor H2AT120
462 phosphorylation are reduced when H4K20me3 is increased, making it unlikely that H3K9
463 or H4K20 methylation impinge on these regulatory mechanisms.

464

465 Instead, our data suggest that disruption of Aurora B localization following targeted
466 recruitment of Suv39 or Suv420 to the centromere may arise due to misregulation of
467 centromere cohesion and/or transcription. As with marks of heterochromatin, cohesin is
468 enriched at pericentromeres (Eckert et al., 2007, Glynn et al., 2004, Weber et al., 2004).
469 This distribution of cohesin is required for transcription of mitotic centromeres such that
470 disruption of either pericentromere cohesin enrichment, or transcription itself, impairs
471 Aurora B localization (Jambhekar et al., 2014, Kleyman et al., 2014, Perea-Resa et al.,
472 2020). Work from our group and others have demonstrated that Suv420-dependent
473 H4K20me3 enhances pericentromeric cohesin (Hahn et al., 2013, Manning et al., 2014,
474 Bernard et al., 2001). This relationship would predict that Suv420-dependent methylation
475 should promote centromere transcription and Aurora B localization. However, we find
476 that following Suv39/Suv420 tethering to centromeres, increased centromere H4K20me3
477 corresponds with reduced, not enhanced, transcript abundance and Aurora B
478 localization at centromeres (Supplemental Figure 6C). Together these data support a
479 model whereby suppression of centromere transcription itself and/or the reduction in
480 centromere transcripts resulting from spreading of H4K20me3 from the pericentromere
481 into the centromere may be sufficient, irrespective of cohesin enrichment, to disrupt CPC
482 localization.

483

484 **Increased H4K20me3 contributes to chromosome instability**

485 The aneuploid chromosome content that results from mitotic segregation errors
486 contributes to infertility, and is a primary cause of non-viable embryos and birth defects

487 (Baker et al., 2009, Choi et al., 2009, Gao et al., 2007, Heilig et al., 2010, Kuukasjarvi et
488 al., 1997, McClelland et al., 2009, Nowell, 1976, Rajagopalan and Lengauer, 2004,
489 Swanton et al., 2009, Sotillo et al., 2010, Cucco and Musio, 2016). Persistent underlying
490 defects in chromosome segregation, termed chromosome instability (CIN), (Baker et al.,
491 2009, Sotillo et al., 2007, Weaver et al., 2007, Hagstrom and Meyer, 2003) are prevalent
492 in cancer contexts where CIN promotes intratumor heterogeneity that in turn contributes
493 to tumor evolution and drug resistance (Baker et al., 2009, Choi et al., 2009, Gao et al.,
494 2007, Heilig et al., 2010, Kuukasjarvi et al., 1997, McClelland et al., 2009, Nowell, 1976,
495 Rajagopalan and Lengauer, 2004, Swanton et al., 2009, Sotillo et al., 2010, Weaver et
496 al., 2007). Merotelic kinetochore attachments are demonstrated to be the primary cause
497 of segregation errors in human cells (Cimini et al., 2001, Cimini et al., 2003, Ganem et
498 al., 2009, Thompson and Compton, 2008), suggesting that corruption of the Aurora B
499 error correction pathway may be prevalent in CIN. Nevertheless, while mutations in
500 genes directly involved in spindle structure, chromosome segregation, or mitotic
501 checkpoints have been associated with a subset of cancers and hereditary disorders
502 (Kim et al., 2012, Chung et al., 2012, Cahill et al., 1998, Cahill et al., 1999, Cucco and
503 Musio, 2016), these mutations do not explain CIN in the vast majority of contexts (Wang
504 et al., 2004, Negrini et al., 2010, Rajagopalan and Lengauer, 2004).

505

506 Our data suggest that changes in centromere methylation may underlie CIN in some
507 cancer contexts. Consistent with this model, our work and others demonstrate that
508 depletion of H3K9 demethylase enzymes, or high expression of H3K9 or H4K20
509 methyltransferase enzymes compromise mitotic fidelity in experimental systems and/or
510 correspond both with aneuploidy and poor outcome in human cancer patients (Figure
511 1B, Supplemental Table 1, (Janssen et al., 2018, Black et al., 2012, Kupershmit et al.,
512 2014, Frescas et al., 2008)). We find centromere tethering of either Suv39 or Suv420 is

513 sufficient to compromise Aurora B kinase localization at centromeres and result in
514 reduced phosphorylation of Aurora B substrates that are critical for proper chromosome
515 segregation. Hec1, a key Aurora B substrate that governs kinetochore microtubule
516 stability and mitotic error correction, is also a substrate for the related Aurora A kinase
517 (DeLuca, 2017). Consistent with this redundant regulation, our data indicate that when
518 centromere methylation is experimentally enhanced, or in cancer contexts where Suv39
519 or Suv420 expression is high and H4K20me3 is therefore likely high, sensitivity to
520 inhibition of both Aurora A and Aurora B kinase is increased (Figure 7). The Aurora
521 kinase family represent promising therapeutic targets that are actively being pursued in
522 clinical and preclinical studies (Tang et al., 2017). Our results propose an intriguing
523 possibility that levels of H4K20me3 (or expression of the enzymes that directly or
524 indirectly promote this methylation state) may be predictive of CIN and may furthermore
525 indicate sensitivity to molecular therapeutics that target Aurora B directly.

526

527 **Methods and Materials:**

528 *Cell Culture, siRNA and transgene expression*

529 hTERT-RPE-1 (RPE-1) cells were grown in Dulbecco's Modified Essential Medium
530 (DMEM). Breast Cancer cell lines HCC1187, HCC202, and ZR-75-1 were grown in
531 RPMI medium, SK-BR-3 were grown in McCoy's 5a medium, and MCF7 grown in
532 Eagles MEM medium. All cell culture medium were supplemented with 10% fetal bovine
533 serum and 1% Penicillin + Streptomycin and cells grown at 37°C with 5% CO₂.

534

535 Depletion of KDM4A was carried out through transient transfection of one of four
536 individual, or a SMARTpool of all four, ON-TARGETplus siRNA constructs (horizon
537 inspired cell solutions) using the RNAiMAX transfection reagent (Invitrogen) according to
538 manufacturer's instructions. Transfection with individual, or a SMARTpool of four, non-

539 targeting siRNA sequences (horizon inspired cell solutions) were used as a negative
540 control for KDM4A depletion. Knockdown efficiency was monitored by qPCR using
541 KDM4A-specific primers. Expression of centromere-targeted, GFP-tagged cen-GFP,
542 cen-Suv39-GFP and cen-Suv420-GFP fusion proteins, and non-targeted Suv420-GFP
543 was achieved by cloning the respective cDNA into Addgene vector CENP-B DBD
544 INCENP GFP (45237, Addgene) at NheI / BamHI. Inducible expression was achieved
545 by cloning the GFP tagged constructs into plvx-Tre3G-IRES (631362, Clonetech) at
546 NotI / NdeI restriction cut sites. Expression vectors were transiently or stably expressed
547 using Lipofectamine 3000 transfection reagent, according to manufacturer's instructions.
548 Inducible expression of transgenes was achieved by the addition of 2 µg/mL Doxycycline
549 for 16-24h. "Mock" controls reflect the individual cell lines in the absence of Doxycycline-
550 induction. Western blot analysis was used to confirm population level expression of each
551 construct. Immunofluorescence for GFP was used to confirm expression and centromere
552 localization for all single cell analyses performed. Sequences for all siRNA constructs
553 and qPCR primers are represented in Supplemental Table 3.

554

555 *Metaphase spreads, fixation, and staining for immunofluorescence imaging*

556 Metaphase spreads were prepared as in (Martins et al., 2016). Mitotic cells were
557 collected by shake off following 3h incubation in 100ng/mL nocodazole, washed briefly in
558 PBS (137mM NaCl, 2.7mM KCl, 10mM Na₂HPO₄, KH₂PO₄) and incubated in 75mM KCl
559 for 12 minutes at 37°C. Cells were spun onto poly L lysine-coated chamber slides at
560 340xg for 5 minutes, then incubated in 37°C KCM buffer (120mM KCl, 20mM NaCl, and
561 10mM Tris HCl pH 8.0, in 0.1% Triton X-100) for 10 minutes.

562

563 For analysis of kinetochore protein localization, untreated (metaphase analysis) or
564 nocodazole treated (prometaphase analysis) cells were prepared as in (Kleyman et al.,

565 2014). Cells were incubated in 3.5% paraformaldehyde for 15min, quenched with
566 500mM ammonium chloride in PBS for 10min, incubated in ice cold methanol for 5min,
567 and washed briefly with PBS. For cen-INCENP-mCherry expression, cells were
568 transiently transfected with Addgene plasmid 45233 36h prior to doxycycline induction of
569 cen-Suv420-GFP expression. For inhibition of Suv420 methyltransferase activity, cells
570 were treated with 200nM A196 concurrent with doxycycline induction of cen-Suv420-
571 GFP expression.

572

573 For metaphase and anaphase analyses of chromosome alignment and segregation,
574 cells were fixed in 4% paraformaldehyde for 20min, washed briefly in PBS, post-
575 extracted in PBS + 0.5% Triton X-100 for 10min, washed briefly in PBS, or alternatively
576 fixed in ice cold methanol for 10min. For analysis of merotelic error correction capacity
577 cells were incubated in the presence of 100 μ M Monastrol for 4hrs, washed twice for
578 5min in drug-free growth medium at 37C, and incubated in growth medium
579 supplemented with 25 μ M MG132 (to prevent anaphase progression) prior to fixation at
580 indicated times. For inhibitor sensitivity assays, cells were treated with indicated
581 concentration of each drug for 12 hours prior to fixation.

582

583 Chromosome spreads were stained with antibodies diluted in KCM + 1%BSA. All other
584 fixation methods were followed by 30min block in TBS-BSA (10mM Tris at pH 7.5,
585 150mM NaCl, 1% bovine serum albumin) + 0.1% Triton X-100 and incubation in primary
586 then secondary antibodies in a humid chamber. Primary and secondary dilutions were
587 made in TBS-BSA + 0.1% Triton X-100. DNA was detected with 0.2 μ g/mL DAPI added
588 to secondary antibody incubations. Coverslips were mounted onto slides using Prolong
589 Antifade Gold (Molecular Probes).

590

591 *Antibodies*

592 The following antibodies were used for immunofluorescence and/or western blot
593 analyses: human anti centromere (ACA) (Antibodies Inc. 15-234); mouse anti H3K9me2
594 (ab1220, Abcam); rabbit anti H3K9me3 (ab176916, Abcam); rabbit anti H3 (ab1791,
595 Abcam); rabbit anti H4K20me3 (ab9053, Abcam); rabbit anti H4 (ab7311, Abcam); rabbit
596 anti H3S10p (04-817, Millipore); mouse anti α -tubulin (dm1 α , Sigma); mouse anti Aurora
597 B (AIM-1, BD Biosciences); rabbit anti H3T3p (97145, Cell Signaling); rabbit anti
598 H2AT120p (61196, Active Motif); rabbit anti CENP-As7p (07-232, Upstate); rabbit anti
599 CENP-A (2186, Cell Signaling); rabbit anti pHEC1S55p (pA5-85846, Invitrogen); mouse
600 anti HEC1 (9G3.23, Novus Biologicals); goat anti GFP (ab6662, Abcam); rabbit anti
601 GFP (2956, Cell Signaling); rabbit anti mCherry (PA5-34974, Invitrogen).

602

603 *Fluorescence Microscopy, Image Analysis, and Statistics*

604 Cells were captured with a Zyla sCMOS camera mounted on a Nikon Ti-E microscope
605 with a 60x Plan Apo oil immersion objective for fixed immunofluorescence, or a 20x CFI
606 Plan Fluor objective for live cell imaging. All images within a single replicate were
607 prepared and imaged in parallel, and images captured using the same exposure time. All
608 single cells or single kinetochore measurements were normalized to the average
609 intensity of the respective control condition and represented as fold-change in
610 fluorescence. For metaphase and anaphase cell analyses, a minimum of 30 mitotic cells
611 were analyzed per condition for each of 3 biological replicates. In these analyses,
612 lagging chromosomes are defined as single chromosomes (marked by ACA-stained
613 kinetochore) that are located between the two masses of segregating chromosomes
614 (anaphase plates) and at least as far from the next nearest kinetochore as the anaphase
615 plate is wide (based on ACA staining). Significance between biological replicates (n=3)

616 was determined using a students' two-tailed t-test. To assess centromere specific
617 protein levels NIS Elements software was used to draw a line through ACA-stained
618 centromere/kinetochore pairs. The intensity of antibody staining along the line was
619 assessed for 3 kinetochore pairs per cell. To assess centromere enrichment, average
620 pixel intensity of H4K20me3 staining was measured in 10 uniform ROIs defined at ACA-
621 stained centromeres/kinetochores per cell and divided by the average H4K20me3
622 staining at ROIs defined on DAPI stained chromatin. Analyses were performed for a
623 minimum of 30 cells in each of 3 biological replicates. Significance between biological
624 replicates (n=3) was determined using a students' two-tailed t-test. Live cell images were
625 captured at 10 coordinates per condition at 5-minute intervals for 24hrs for each of 3
626 biological replicates. Mitotic timing was recorded from NEB until anaphase onset
627 (Mercadante et al., 2019) for a minimum of 50 cells per replicate and significance
628 between biological replicates (n=3) was determined using a students' two-tailed t-test. All
629 analyses were performed on unprocessed images. For publication images NIS elements
630 deconvolution software was used. All images within a single panel were cropped
631 comparably using ImageJ software to allow for direct comparison.

632

633 *qPCR analysis of centromere transcript abundance*

634 RPE-1 cells carrying the inducible cen-Suv39-GFP or cen-Suv420-GFP construct were
635 plated in cell culture flasks and induced, or not, with 2 µg/mL Doxycycline for 24h. 100
636 ng/mL Nocodazole was added to the growth medium for the last 4 hours of induction.
637 Mitotic cells were collected via manual shake off. RNA was isolated with Trizol and
638 purified using Qiagen's RNeasy columns. Purified RNA was quantitated by qPCR per
639 the double delta Ct method that considers transcript changes relative to an internal
640 control that is insensitive to the experimental manipulations (in this case GAPDH
641 transcript), using transcript-specific primers (see Supplemental Table 3), a ABI 7500,

642 and power up SYBR Green Master mix (Roche). Primers for centromere α satellite
643 transcripts were previously described (Liu et al., 2015, Xue et al., 2013).

644

645 *Gene Expression, Aneuploidy Correlation, Patient Survival, and Drug Sensitivity*
646 *Analyses*

647 For analyses of Suv39 and Suv420 isoform expression in cancer rna-seq2 illumina
648 hiseq RSEM normalized data was acquired through FireBrowse (firebrowse.org) and
649 aneuploidy scores obtained from (Taylor et al., 2018). Both datasets were imported into
650 an R statistical programming environment version 3.3.1 and run through a custom
651 analysis pipeline to reformat and combine the datasets based on tumor sample. The
652 Pearson correlation coefficient between aneuploidy score and gene expression was
653 determined as described in (Taylor et al., 2018) and linear regression analysis
654 performed to determine statistical significance where a p value of < 0.0025 reflects a
655 significant correlation. RPKM-normalized expression values of Suv39 and Suv420
656 isoforms in normal and cancer contexts were obtained from FireBrowse and filtered to
657 select and graph only cancer subtypes where paired normal tissue samples were
658 available. The Kaplan-Meier Plotter platform (kmplot.com/analysis; (Nagy et al., 2018,
659 Györfy et al., 2010)) was used to query survival data relative to Suv39 and Suv420
660 isoform expression to compare samples for top and bottom quartile expression for their
661 respective genes. Hochberg's step-up method corrected p values where determined and
662 significance defined as $p \leq 0.0053$. Gene expression data was downloaded from the
663 Broad Cancer Cell Line Encyclopedia (CCLE) January 02, 2019 run containing
664 expression data of 84,434 genes from 1,457 different cancer cell lines. Drug Screening
665 IC50 AUC (area under the fitted dose response curve) data was downloaded from the
666 Genomics of Drug Sensitivity in Cancer database GDSC1 run containing 518 different
667 drugs across 988 different cell lines. Both sets of data were then imported into an R

668 statistical programming environment version 3.3.1 and run through an analysis pipeline
669 to reformat and combine the datasets based on cancer cell lines present in both. The
670 data sets were sorted to independently identify the top and bottom quartile in terms of
671 Suv39 or Suv420 expression. For both the high and low expression groups for each
672 gene, the drug IC50 of each individual cell line and the mean +/- SEM of all cell lines in
673 each group were graphed for each drug of interest. Significance was determined using a
674 students' two tailed t-test corrected for multiple comparisons using the Bonferroni
675 correction method where $p < 0.00625$ is significant.

676

677 **Acknowledgements**

678 We thank members of the Manning lab for critical reading and feedback on this
679 manuscript. This work was supported by a Smith Family Award for Excellence in
680 Biomedical Research and R00CA182731 to ALM.

681

682 The authors declare no competing interests.

683

684 **Author Contributions**

685 AL Manning and CP Herlihy conceived and designed the experiments. CP Herlihy, S
686 Hahn, E Crowley, and NM Hermance performed the experiments. AL Manning and CP
687 Herlihy wrote the manuscript with input and approval from all authors.

688

689 **References**

690 ABE, Y., SAKO, K., TAKAGAKI, K., HIRAYAMA, Y., UCHIDA, K. S., HERMAN, J. A.,
691 DELUCA, J. G. & HIROTA, T. 2016. HP1-Assisted Aurora B Kinase Activity
692 Prevents Chromosome Segregation Errors. *Dev Cell*, 36, 487-97.
693 BAKER, D. J., JIN, F., JEGANATHAN, K. B. & VAN DEURSEN, J. M. 2009. Whole
694 chromosome instability caused by Bub1 insufficiency drives tumorigenesis

- 695 through tumor suppressor gene loss of heterozygosity. *Cancer Cell*, 16, 475-
696 86.
- 697 BARNHART, M. C., KUICH, P. H., STELLFOX, M. E., WARD, J. A., BASSETT, E. A., BLACK,
698 B. E. & FOLTZ, D. R. 2011. HJURP is a CENP-A chromatin assembly factor
699 sufficient to form a functional de novo kinetochore. *J Cell Biol*, 194, 229-43.
- 700 BERNARD, P., MAURE, J. F., PARTRIDGE, J. F., GENIER, S., JAVERZAT, J. P. &
701 ALLSHIRE, R. C. 2001. Requirement of heterochromatin for cohesion at
702 centromeres. *Science*, 294, 2539-42.
- 703 BERRY, W. L. & JANKNECHT, R. 2013. KDM4/JMJD2 histone demethylases:
704 epigenetic regulators in cancer cells. *Cancer Res*, 73, 2936-42.
- 705 BLACK, J. C., VAN RECHEM, C. & WHETSTINE, J. R. 2012. Histone lysine methylation
706 dynamics: establishment, regulation, and biological impact. *Mol Cell*, 48, 491-
707 507.
- 708 BLOWER, M. D. 2016. Centromeric Transcription Regulates Aurora-B Localization
709 and Activation. *Cell Rep*, 15, 1624-33.
- 710 BROAD, A. J., DELUCA, K. F. & DELUCA, J. G. 2020. Aurora B kinase is recruited to
711 multiple discrete kinetochore and centromere regions in human cells. *J Cell*
712 *Biol*, 219.
- 713 BROMBERG, K. D., MITCHELL, T. R., UPADHYAY, A. K., JAKOB, C. G., JHALA, M. A.,
714 COMESS, K. M., LASKO, L. M., LI, C., TUZON, C. T., DAI, Y., LI, F., ERAM, M. S.,
715 NUBER, A., SONI, N. B., MANAVES, V., ALGIRE, M. A., SWEIS, R. F., TORRENT,
716 M., SCHOTTA, G., SUN, C., MICHAELIDES, M. R., SHOEMAKER, A. R.,
717 ARROWSMITH, C. H., BROWN, P. J., SANTHAKUMAR, V., MARTIN, A., RICE, J.
718 C., CHIANG, G. G., VEDADI, M., BARSYTE-LOVEJOY, D. & PAPPANO, W. N.
719 2017. The SUV4-20 inhibitor A-196 verifies a role for epigenetics in genomic
720 integrity. *Nat Chem Biol*, 13, 317-324.
- 721 CAHILL, D. P., DA COSTA, L. T., CARSON-WALTER, E. B., KINZLER, K. W.,
722 VOGELSTEIN, B. & LENGAUER, C. 1999. Characterization of MAD2B and other
723 mitotic spindle checkpoint genes. *Genomics*, 58, 181-7.
- 724 CAHILL, D. P., LENGAUER, C., YU, J., RIGGINS, G. J., WILLSON, J. K., MARKOWITZ, S. D.,
725 KINZLER, K. W. & VOGELSTEIN, B. 1998. Mutations of mitotic checkpoint
726 genes in human cancers. *Nature*, 392, 300-3.
- 727 CARRETERO, M., RUIZ-TORRES, M., RODRIGUEZ-CORSINO, M., BARTHELEMY, I. &
728 LOSADA, A. 2013. Pds5B is required for cohesion establishment and Aurora B
729 accumulation at centromeres. *EMBO J*, 32, 2938-49.
- 730 CARROLL, C. W. & STRAIGHT, A. F. 2006. Centromere formation: from epigenetics to
731 self-assembly. *Trends Cell Biol*, 16, 70-8.
- 732 CHEESEMAN, I. M., CHAPPIE, J. S., WILSON-KUBALEK, E. M. & DESAI, A. 2006. The
733 conserved KMN network constitutes the core microtubule-binding site of the
734 kinetochore. *Cell*, 127, 983-97.
- 735 CHOI, C. M., SEO, K. W., JANG, S. J., OH, Y. M., SHIM, T. S., KIM, W. S., LEE, D. S. & LEE, S.
736 D. 2009. Chromosomal instability is a risk factor for poor prognosis of
737 adenocarcinoma of the lung: Fluorescence in situ hybridization analysis of
738 paraffin-embedded tissue from Korean patients. *Lung Cancer*, 64, 66-70.

- 739 CHUNG, N. G., KIM, M. S., YOO, N. J. & LEE, S. H. 2012. Somatic mutation of STAG2, an
740 aneuploidy-related gene, is rare in acute leukemias. *Leukemia & lymphoma*,
741 53, 1234-5.
- 742 CIMINI, D., HOWELL, B., MADDOX, P., KHODJAKOV, A., DEGRASSI, F. & SALMON, E. D.
743 2001. Merotelic kinetochore orientation is a major mechanism of aneuploidy
744 in mitotic mammalian tissue cells. *J Cell Biol*, 153, 517-27.
- 745 CIMINI, D., MOREE, B., CANMAN, J. C. & SALMON, E. D. 2003. Merotelic kinetochore
746 orientation occurs frequently during early mitosis in mammalian tissue cells
747 and error correction is achieved by two different mechanisms. *J Cell Sci*, 116,
748 4213-25.
- 749 CIMINI, D., WAN, X., HIREL, C. B. & SALMON, E. D. 2006. Aurora kinase promotes
750 turnover of kinetochore microtubules to reduce chromosome segregation
751 errors. *Curr Biol*, 16, 1711-8.
- 752 CUCCO, F. & MUSIO, A. 2016. Genome stability: What we have learned from
753 cohesinopathies. *Am J Med Genet C Semin Med Genet*, 172, 171-8.
- 754 CUELLAR, T. L., HERZNER, A. M., ZHANG, X., GOYAL, Y., WATANABE, C., FRIEDMAN,
755 B. A., JANAKIRAMAN, V., DURINCK, S., STINSON, J., ARNOTT, D., CHEUNG, T.
756 K., CHAUDHURI, S., MODRUSAN, Z., DOERR, J. M., CLASSON, M. & HALEY, B.
757 2017. Silencing of retrotransposons by SETDB1 inhibits the interferon
758 response in acute myeloid leukemia. *J Cell Biol*, 216, 3535-3549.
- 759 DAI, J., SULLIVAN, B. A. & HIGGINS, J. M. 2006. Regulation of mitotic chromosome
760 cohesion by Haspin and Aurora B. *Dev Cell*, 11, 741-50.
- 761 DAVOLI, T., XU, A. W., MENGWASSER, K. E., SACK, L. M., YOON, J. C., PARK, P. J. &
762 ELLEDGE, S. J. 2013. Cumulative haploinsufficiency and triplosensitivity drive
763 aneuploidy patterns and shape the cancer genome. *Cell*, 155, 948-62.
- 764 DE ROP, V., PADEGANEH, A. & MADDOX, P. S. 2012. CENP-A: the key player behind
765 centromere identity, propagation, and kinetochore assembly. *Chromosoma*,
766 121, 527-38.
- 767 DELUCA, J. G. 2017. Aurora A Kinase Function at Kinetochores. *Cold Spring Harb*
768 *Symp Quant Biol*, 82, 91-99.
- 769 DELUCA, J. G., GALL, W. E., CIFERRI, C., CIMINI, D., MUSACCHIO, A. & SALMON, E. D.
770 2006. Kinetochore microtubule dynamics and attachment stability are
771 regulated by Hec1. *Cell*, 127, 969-82.
- 772 DELUCA, K. F., LENS, S. M. & DELUCA, J. G. 2011. Temporal changes in Hec1
773 phosphorylation control kinetochore-microtubule attachment stability
774 during mitosis. *J Cell Sci*, 124, 622-34.
- 775 DITCHFIELD, C., JOHNSON, V. L., TIGHE, A., ELLSTON, R., HAWORTH, C., JOHNSON,
776 T., MORTLOCK, A., KEEN, N. & TAYLOR, S. S. 2003. Aurora B couples
777 chromosome alignment with anaphase by targeting BubR1, Mad2, and Cenp-
778 E to kinetochores. *J Cell Biol*, 161, 267-80.
- 779 ECKERT, C. A., GRAVDAHL, D. J. & MEGEE, P. C. 2007. The enhancement of
780 pericentromeric cohesin association by conserved kinetochore components
781 promotes high-fidelity chromosome segregation and is sensitive to
782 microtubule-based tension. *Genes Dev*, 21, 278-91.

- 783 FIORINIELLO, S., MARANO, D., FIORILLO, F., D'ESPOSITO, M. & DELLA RAGIONE, F.
784 2020. Epigenetic Factors That Control Pericentric Heterochromatin
785 Organization in Mammals. *Genes (Basel)*, 11.
- 786 FISCHLE, W., TSENG, B. S., DORMANN, H. L., UEBERHEIDE, B. M., GARCIA, B. A.,
787 SHABANOWITZ, J., HUNT, D. F., FUNABIKI, H. & ALLIS, C. D. 2005. Regulation
788 of HP1-chromatin binding by histone H3 methylation and phosphorylation.
789 *Nature*, 438, 1116-22.
- 790 FRESCAS, D., GUARDAVACCARO, D., KUCHAY, S. M., KATO, H., POLESHKO, A.,
791 BASRUR, V., ELENITOBA-JOHNSON, K. S., KATZ, R. A. & PAGANO, M. 2008.
792 KDM2A represses transcription of centromeric satellite repeats and
793 maintains the heterochromatic state. *Cell Cycle*, 7, 3539-47.
- 794 GANEM, N. J., GODINHO, S. A. & PELLMAN, D. 2009. A mechanism linking extra
795 centrosomes to chromosomal instability. *Nature*, 460, 278-82.
- 796 GAO, C., FURGE, K., KOEMAN, J., DYKEMA, K., SU, Y., CUTLER, M. L., WERTS, A., HAAK,
797 P. & VANDE WOUDE, G. F. 2007. Chromosome instability, chromosome
798 transcriptome, and clonal evolution of tumor cell populations. *Proc Natl Acad
799 Sci U S A*, 104, 8995-9000.
- 800 GHANDI, M., HUANG, F. W., JANÉ-VALBUENA, J., KRYUKOV, G. V., LO, C. C.,
801 MCDONALD, E. R., BARRETINA, J., GELFAND, E. T., BIELSKI, C. M., LI, H., HU,
802 K., ANDREEV-DRAKHLIN, A. Y., KIM, J., HESS, J. M., HAAS, B. J., AGUET, F.,
803 WEIR, B. A., ROTHBERG, M. V., PAOLELLA, B. R., LAWRENCE, M. S., AKBANI,
804 R., LU, Y., TIV, H. L., GOKHALE, P. C., DE WECK, A., MANSOUR, A. A., OH, C.,
805 SHIH, J., HADI, K., ROSEN, Y., BISTLINE, J., VENKATESAN, K., REDDY, A.,
806 SONKIN, D., LIU, M., LEHAR, J., KORN, J. M., PORTER, D. A., JONES, M. D., GOLJI,
807 J., CAPONIGRO, G., TAYLOR, J. E., DUNNING, C. M., CREECH, A. L., WARREN, A.
808 C., MCFARLAND, J. M., ZAMANIGHOMI, M., KAUFFMANN, A., STRANSKY, N.,
809 IMIELINSKI, M., MARUVKA, Y. E., CHERNIACK, A. D., TSHERNIAK, A.,
810 VAZQUEZ, F., JAFFE, J. D., LANE, A. A., WEINSTOCK, D. M., JOHANNESSEN, C.
811 M., MORRISSEY, M. P., STEGMEIER, F., SCHLEGEL, R., HAHN, W. C., GETZ, G.,
812 MILLS, G. B., BOEHM, J. S., GOLUB, T. R., GARRAWAY, L. A. & SELLERS, W. R.
813 2019. Next-generation characterization of the Cancer Cell Line Encyclopedia.
814 *Nature*, 569, 503-508.
- 815 GLYNN, E. F., MEGEE, P. C., YU, H. G., MISTROT, C., UNAL, E., KOSHLAND, D. E.,
816 DERISI, J. L. & GERTON, J. L. 2004. Genome-wide mapping of the cohesin
817 complex in the yeast *Saccharomyces cerevisiae*. *PLoS Biol*, 2, E259.
- 818 GREGAN, J., POLAKOVA, S., ZHANG, L., TOLIĆ-NØRRELYKKE, I. M. & CIMINI, D. 2011.
819 Merotelic kinetochore attachment: causes and effects. *Trends Cell Biol*, 21,
820 374-81.
- 821 GULER, G. D., TINDELL, C. A., PITTI, R., WILSON, C., NICHOLS, K., KAIWAI CHEUNG,
822 T., KIM, H. J., WONGCHENKO, M., YAN, Y., HALEY, B., CUELLAR, T., WEBSTER,
823 J., ALAG, N., HEGDE, G., JACKSON, E., NANCE, T. L., GIRESI, P. G., CHEN, K. B.,
824 LIU, J., JHUNJHUNWALA, S., SETTLEMAN, J., STEPHAN, J. P., ARNOTT, D. &
825 CLASSON, M. 2017. Repression of Stress-Induced LINE-1 Expression Protects
826 Cancer Cell Subpopulations from Lethal Drug Exposure. *Cancer Cell*, 32, 221-
827 237.e13.

- 828 GUSE, A., CARROLL, C. W., MOREE, B., FULLER, C. J. & STRAIGHT, A. F. 2011. In vitro
829 centromere and kinetochore assembly on defined chromatin templates.
830 *Nature*, 477, 354-8.
- 831 GYÖRFFY, B., LANCKY, A., EKLUND, A. C., DENKERT, C., BUDCZIES, J., LI, Q. &
832 SZALLASI, Z. 2010. An online survival analysis tool to rapidly assess the effect
833 of 22,277 genes on breast cancer prognosis using microarray data of 1,809
834 patients. *Breast Cancer Res Treat*, 123, 725-31.
- 835 HADDERS, M. A., HINDRIKSEN, S., TRUONG, M. A., MHASKAR, A. N., WOPKEN, J. P.,
836 VROMANS, M. J. M. & LENS, S. M. A. 2020. Untangling the contribution of
837 Haspin and Bub1 to Aurora B function during mitosis. *J Cell Biol*, 219.
- 838 HAGSTROM, K. A. & MEYER, B. J. 2003. Condensin and cohesin: more than
839 chromosome compactor and glue. *Nat Rev Genet*, 4, 520-34.
- 840 HAHN, M., DAMBACHER, S., DULEV, S., KUZNETSOVA, A. Y., ECK, S., WORZ, S., SADIC,
841 D., SCHULTE, M., MALLM, J. P., MAISER, A., DEBS, P., VON MELCHNER, H.,
842 LEONHARDT, H., SCHERMELLEH, L., ROHR, K., RIPPE, K., STORCHOVA, Z. &
843 SCHOTTA, G. 2013. Suv4-20h2 mediates chromatin compaction and is
844 important for cohesin recruitment to heterochromatin. *Genes & development*,
845 27, 859-72.
- 846 HAUF, S., COLE, R. W., LATERRA, S., ZIMMER, C., SCHNAPP, G., WALTER, R., HECKEL,
847 A., VAN MEEL, J., RIEDER, C. L. & PETERS, J. M. 2003. The small molecule
848 Hesperadin reveals a role for Aurora B in correcting kinetochore-
849 microtubule attachment and in maintaining the spindle assembly checkpoint.
850 *J Cell Biol*, 161, 281-94.
- 851 HEILIG, C. E., LOFFLER, H., MAHLKNECHT, U., JANSSEN, J. W., HO, A. D., JAUCH, A. &
852 KRAMER, A. 2010. Chromosomal instability correlates with poor outcome in
853 patients with myelodysplastic syndromes irrespectively of the cytogenetic
854 risk group. *J Cell Mol Med*, 14, 895-902.
- 855 HINDRIKSEN, S., LENS, S. M. A. & HADDERS, M. A. 2017. The Ins and Outs of Aurora
856 B Inner Centromere Localization. *Front Cell Dev Biol*, 5, 112.
- 857 HINSHAW, S. M. & HARRISON, S. C. 2018. Kinetochore Function from the Bottom Up.
858 *Trends Cell Biol*, 28, 22-33.
- 859 HIROTA, T., LIPP, J. J., TOH, B. H. & PETERS, J. M. 2005. Histone H3 serine 10
860 phosphorylation by Aurora B causes HP1 dissociation from heterochromatin.
861 *Nature*, 438, 1176-80.
- 862 HUANG, H., LAMPSON, M., EFIMOV, A. & YEN, T. J. 2018. Chromosome instability in
863 tumor cells due to defects in Aurora B mediated error correction at
864 kinetochores. *Cell Cycle*, 17, 2622-2636.
- 865 IDEUE, T., CHO, Y., NISHIMURA, K. & TANI, T. 2014. Involvement of satellite I
866 noncoding RNA in regulation of chromosome segregation. *Genes Cells*, 19,
867 528-38.
- 868 JAMBHEKAR, A., EMERMAN, A. B., SCHWEIDENBACK, C. T. & BLOWER, M. D. 2014.
869 RNA stimulates Aurora B kinase activity during mitosis. *PLoS One*, 9,
870 e100748.
- 871 JANSSEN, A., COLMENARES, S. U. & KARPEN, G. H. 2018. Heterochromatin: Guardian
872 of the Genome. *Annu Rev Cell Dev Biol*, 34, 265-288.

- 873 KALLIO, M. J., MCCLELAND, M. L., STUKENBERG, P. T. & GORBSKY, G. J. 2002.
874 Inhibition of aurora B kinase blocks chromosome segregation, overrides the
875 spindle checkpoint, and perturbs microtubule dynamics in mitosis. *Curr Biol*,
876 12, 900-5.
- 877 KANG, J., CHAUDHARY, J., DONG, H., KIM, S., BRAUTIGAM, C. A. & YU, H. 2011. Mitotic
878 centromeric targeting of HP1 and its binding to Sgo1 are dispensable for
879 sister-chromatid cohesion in human cells. *Mol Biol Cell*, 22, 1181-90.
- 880 KAPOOR, T. M., MAYER, T. U., COUGHLIN, M. L. & MITCHISON, T. J. 2000. Probing
881 spindle assembly mechanisms with monastrol, a small molecule inhibitor of
882 the mitotic kinesin, Eg5. *J Cell Biol*, 150, 975-88.
- 883 KELLY, A. E., GHENOIU, C., XUE, J. Z., ZIERHUT, C., KIMURA, H. & FUNABIKI, H. 2010.
884 Survivin reads phosphorylated histone H3 threonine 3 to activate the mitotic
885 kinase Aurora B. *Science*, 330, 235-9.
- 886 KIM, M. S., KIM, S. S., JE, E. M., YOO, N. J. & LEE, S. H. 2012. Mutational and
887 expressional analyses of STAG2 gene in solid cancers. *Neoplasma*, 59, 524-9.
- 888 KLEYMAN, M., KABECHE, L. & COMPTON, D. A. 2014. STAG2 promotes error
889 correction in mitosis by regulating kinetochore-microtubule attachments. *J*
890 *Cell Sci*, 127, 4225-33.
- 891 KRENN, V. & MUSACCHIO, A. 2015. The Aurora B Kinase in Chromosome Bi-
892 Orientation and Spindle Checkpoint Signaling. *Front Oncol*, 5, 225.
- 893 KUPERSHMIT, I., KHOURY-HADDAD, H., AWWAD, S. W., GUTTMANN-RAVIV, N. &
894 AYOUB, N. 2014. KDM4C (GASC1) lysine demethylase is associated with
895 mitotic chromatin and regulates chromosome segregation during mitosis.
896 *Nucleic Acids Res*, 42, 6168-82.
- 897 KUUKASJARVI, T., KARHU, R., TANNER, M., KAHKONEN, M., SCHAFFER, A.,
898 NUPPONEN, N., PENNANEN, S., KALLIONIEMI, A., KALLIONIEMI, O. P. &
899 ISOLA, J. 1997. Genetic heterogeneity and clonal evolution underlying
900 development of asynchronous metastasis in human breast cancer. *Cancer*
901 *Res*, 57, 1597-604.
- 902 LAM, A. L., BOIVIN, C. D., BONNEY, C. F., RUDD, M. K. & SULLIVAN, B. A. 2006. Human
903 centromeric chromatin is a dynamic chromosomal domain that can spread
904 over noncentromeric DNA. *Proc Natl Acad Sci U S A*, 103, 4186-91.
- 905 LAMPSON, M. A., RENDUCHITALA, K., KHODJAKOV, A. & KAPOOR, T. M. 2004.
906 Correcting improper chromosome-spindle attachments during cell division.
907 *Nat Cell Biol*, 6, 232-7.
- 908 LIANG, C., ZHANG, Z., CHEN, Q., YAN, H., ZHANG, M., ZHOU, L., XU, J., LU, W. & WANG,
909 F. 2020. Centromere-localized Aurora B kinase is required for the fidelity of
910 chromosome segregation. *J Cell Biol*, 219.
- 911 LIU, H., QU, Q., WARRINGTON, R., RICE, A., CHENG, N. & YU, H. 2015. Mitotic
912 Transcription Installs Sgo1 at Centromeres to Coordinate Chromosome
913 Segregation. *Mol Cell*, 59, 426-36.
- 914 LIU, Y., CHEN, C., XU, Z., SCUOPPO, C., RILLAHAN, C. D., GAO, J., SPITZER, B.,
915 BOSBACH, B., KASTENHUBER, E. R., BASLAN, T., ACKERMANN, S., CHENG, L.,
916 WANG, Q., NIU, T., SCHULTZ, N., LEVINE, R. L., MILLS, A. A. & LOWE, S. W.
917 2016. Deletions linked to TP53 loss drive cancer through p53-independent
918 mechanisms. *Nature*, 531, 471-475.

- 919 MANNING, A. L., YAZINSKI, S. A., NICOLAY, B., BRYLL, A., ZOU, L. & DYSON, N. J. 2014.
920 Suppression of genome instability in pRB-deficient cells by enhancement of
921 chromosome cohesion. *Mol Cell*, 53, 993-1004.
- 922 MARTINS, N. M., BERGMANN, J. H., SHONO, N., KIMURA, H., LARIONOV, V.,
923 MASUMOTO, H. & EARNSHAW, W. C. 2016. Epigenetic engineering shows
924 that a human centromere resists silencing mediated by H3K27me3/K9me3.
925 *Mol Biol Cell*, 27, 177-96.
- 926 MARTINS, N. M. C., CISNEROS-SOBERANIS, F., PESENTI, E., KOCHANOVA, N. Y.,
927 SHANG, W. H., HORI, T., NAGASE, T., KIMURA, H., LARIONOV, V., MASUMOTO,
928 H., FUKAGAWA, T. & EARNSHAW, W. C. 2020. H3K9me3 maintenance on a
929 human artificial chromosome is required for segregation but not centromere
930 epigenetic memory. *J Cell Sci*, 133.
- 931 MCCLELLAND, S. E., BURRELL, R. A. & SWANTON, C. 2009. Chromosomal instability:
932 a composite phenotype that influences sensitivity to chemotherapy. *Cell*
933 *Cycle*, 8, 3262-6.
- 934 MEPELINK, A., KABECHE, L., VROMANS, M. J., COMPTON, D. A. & LENS, S. M. 2015.
935 Shugoshin-1 balances Aurora B kinase activity via PP2A to promote
936 chromosome bi-orientation. *Cell Rep*, 11, 508-15.
- 937 MERCADANTE, D. L., CROWLEY, E. A. & MANNING, A. L. 2019. Live Cell Imaging to
938 Assess the Dynamics of Metaphase Timing and Cell Fate Following Mitotic
939 Spindle Perturbations. *J Vis Exp*.
- 940 MURO, Y., MASUMOTO, H., YODA, K., NOZAKI, N., OHASHI, M. & OKAZAKI, T. 1992.
941 Centromere protein B assembles human centromeric alpha-satellite DNA at
942 the 17-bp sequence, CENP-B box. *J Cell Biol*, 116, 585-96.
- 943 NAGY, Á., LÁNCZKY, A., MENYHÁRT, O. & GYÓRFFY, B. 2018. Validation of miRNA
944 prognostic power in hepatocellular carcinoma using expression data of
945 independent datasets. *Sci Rep*, 8, 9227.
- 946 NEGRINI, S., GORGOULIS, V. G. & HALAZONETIS, T. D. 2010. Genomic instability--an
947 evolving hallmark of cancer. *Nature reviews. Molecular cell biology*, 11, 220-8.
- 948 NOWELL, P. C. 1976. The clonal evolution of tumor cell populations. *Science*, 194,
949 23-8.
- 950 O'CARROLL, D., SCHERTHAN, H., PETERS, A. H., OPRAVIL, S., HAYNES, A. R., LAIBLE,
951 G., REA, S., SCHMID, M., LEBERSORGER, A., JERRATSCH, M., SATTLER, L.,
952 MATTEI, M. G., DENNY, P., BROWN, S. D., SCHWEIZER, D. & JENUWEIN, T.
953 2000. Isolation and characterization of Suv39h2, a second histone H3
954 methyltransferase gene that displays testis-specific expression. *Mol Cell Biol*,
955 20, 9423-33.
- 956 OHZEKI, J., BERGMANN, J. H., KOUPRINA, N., NOSKOV, V. N., NAKANO, M., KIMURA,
957 H., EARNSHAW, W. C., LARIONOV, V. & MASUMOTO, H. 2012. Breaking the
958 HAC Barrier: histone H3K9 acetyl/methyl balance regulates CENP-A
959 assembly. *EMBO J*, 31, 2391-402.
- 960 OHZEKI, J., LARIONOV, V., EARNSHAW, W. C. & MASUMOTO, H. 2019. De novo
961 formation and epigenetic maintenance of centromere chromatin. *Curr Opin*
962 *Cell Biol*, 58, 15-25.

- 963 PEREA-RESA, C., BURY, L., CHEESEMAN, I. M. & BLOWER, M. D. 2020. Cohesin
964 Removal Reprograms Gene Expression upon Mitotic Entry. *Mol Cell*, 78, 127-
965 140 e7.
- 966 PFAU, S. J. & AMON, A. 2012. Chromosomal instability and aneuploidy in cancer:
967 from yeast to man. *EMBO Rep*, 13, 515-27.
- 968 PLUTA, A. F., SAITOH, N., GOLDBERG, I. & EARNSHAW, W. C. 1992. Identification of a
969 subdomain of CENP-B that is necessary and sufficient for localization to the
970 human centromere. *J Cell Biol*, 116, 1081-93.
- 971 RAJAGOPALAN, H. & LENGAUER, C. 2004. Aneuploidy and cancer. *Nature*, 432, 338-
972 41.
- 973 SCHOTTA, G., LACHNER, M., SARMA, K., EBERT, A., SENGUPTA, R., REUTER, G.,
974 REINBERG, D. & JENUWEIN, T. 2004. A silencing pathway to induce H3-K9
975 and H4-K20 trimethylation at constitutive heterochromatin. *Genes Dev*, 18,
976 1251-62.
- 977 SHARMA, A. B., DIMITROV, S., HAMICHE, A. & VAN DYCK, E. 2019. Centromeric and
978 ectopic assembly of CENP-A chromatin in health and cancer: old marks and
979 new tracks. *Nucleic Acids Res*, 47, 1051-1069.
- 980 SOTILLO, R., HERNANDO, E., DIAZ-RODRIGUEZ, E., TERUYA-FELDSTEIN, J.,
981 CORDON-CARDO, C., LOWE, S. W. & BENEZRA, R. 2007. Mad2 overexpression
982 promotes aneuploidy and tumorigenesis in mice. *Cancer Cell*, 11, 9-23.
- 983 SOTILLO, R., SCHVARTZMAN, J. M., SOCCI, N. D. & BENEZRA, R. 2010. Mad2-induced
984 chromosome instability leads to lung tumour relapse after oncogene
985 withdrawal. *Nature*, 464, 436-40.
- 986 SULLIVAN, B. A. & KARPEN, G. H. 2004. Centromeric chromatin exhibits a histone
987 modification pattern that is distinct from both euchromatin and
988 heterochromatin. *Nat Struct Mol Biol*, 11, 1076-83.
- 989 SWANTON, C., NICKE, B., SCHUETT, M., EKLUND, A. C., NG, C., LI, Q., HARDCASTLE,
990 T., LEE, A., ROY, R., EAST, P., KSCHISCHO, M., ENDESFELDER, D., WYLIE, P.,
991 KIM, S. N., CHEN, J. G., HOWELL, M., RIED, T., HABERMANN, J. K., AUER, G.,
992 BRENTON, J. D., SZALLASI, Z. & DOWNWARD, J. 2009. Chromosomal
993 instability determines taxane response. *Proc Natl Acad Sci U S A*, 106, 8671-6.
- 994 TANG, A., GAO, K., CHU, L., ZHANG, R., YANG, J. & ZHENG, J. 2017. Aurora kinases:
995 novel therapy targets in cancers. *Oncotarget*, 8, 23937-23954.
- 996 TAYLOR, A. M., SHIH, J., HA, G., GAO, G. F., ZHANG, X., BERGER, A. C., SCHUMACHER,
997 S. E., WANG, C., HU, H., LIU, J., LAZAR, A. J., CHERNIACK, A. D., BEROUKHIM, R.,
998 MEYERSON, M. & NETWORK, C. G. A. R. 2018. Genomic and Functional
999 Approaches to Understanding Cancer Aneuploidy. *Cancer Cell*, 33, 676-
1000 689.e3.
- 1001 THOMAS, G. E., RENJITH, M. R. & MANNA, T. K. 2017. Kinetochore-microtubule
1002 interactions in chromosome segregation: lessons from yeast and mammalian
1003 cells. *Biochem J*, 474, 3559-3577.
- 1004 THOMPSON, S. L. & COMPTON, D. A. 2008. Examining the link between
1005 chromosomal instability and aneuploidy in human cells. *J Cell Biol*, 180, 665-
1006 72.

- 1007 TSANG, L. W., HU, N. & UNDERHILL, D. A. 2010. Comparative analyses of SUV420H1
1008 isoforms and SUV420H2 reveal differences in their cellular localization and
1009 effects on myogenic differentiation. *PLoS One*, 5, e14447.
- 1010 TSUKAHARA, T., TANNO, Y. & WATANABE, Y. 2010. Phosphorylation of the CPC by
1011 Cdk1 promotes chromosome bi-orientation. *Nature*, 467, 719-23.
- 1012 WANG, E., BALLISTER, E. R. & LAMPSON, M. A. 2011. Aurora B dynamics at
1013 centromeres create a diffusion-based phosphorylation gradient. *J Cell Biol*,
1014 194, 539-49.
- 1015 WANG, F., DAI, J., DAUM, J. R., NIEDZIALKOWSKA, E., BANERJEE, B., STUKENBERG, P.
1016 T., GORBSKY, G. J. & HIGGINS, J. M. 2010. Histone H3 Thr-3 phosphorylation
1017 by Haspin positions Aurora B at centromeres in mitosis. *Science*, 330, 231-5.
- 1018 WANG, Z., CUMMINS, J. M., SHEN, D., CAHILL, D. P., JALLEPALLI, P. V., WANG, T. L.,
1019 PARSONS, D. W., TRAVERSO, G., AWAD, M., SILLIMAN, N., PTAK, J., SZABO, S.,
1020 WILLSON, J. K., MARKOWITZ, S. D., GOLDBERG, M. L., KARESS, R., KINZLER, K.
1021 W., VOGELSTEIN, B., VELCULESCU, V. E. & LENGAUER, C. 2004. Three classes
1022 of genes mutated in colorectal cancers with chromosomal instability. *Cancer*
1023 *research*, 64, 2998-3001.
- 1024 WEAVER, B. A., SILK, A. D., MONTAGNA, C., VERDIER-PINARD, P. & CLEVELAND, D.
1025 W. 2007. Aneuploidy acts both oncogenically and as a tumor suppressor.
1026 *Cancer Cell*, 11, 25-36.
- 1027 WEBER, S. A., GERTON, J. L., POLANCIC, J. E., DERISI, J. L., KOSHLAND, D. & MEGEE, P.
1028 C. 2004. The kinetochore is an enhancer of pericentric cohesin binding. *PLoS*
1029 *Biol*, 2, E260.
- 1030 WELBURN, J. P., VLEUGEL, M., LIU, D., YATES, J. R., LAMPSON, M. A., FUKAGAWA, T.
1031 & CHEESEMAN, I. M. 2010. Aurora B phosphorylates spatially distinct targets
1032 to differentially regulate the kinetochore-microtubule interface. *Mol Cell*, 38,
1033 383-92.
- 1034 XUE, J., WIJERATNE, S. S. & ZEMPLIENI, J. 2013. Holocarboxylase synthetase
1035 synergizes with methyl CpG binding protein 2 and DNA methyltransferase 1
1036 in the transcriptional repression of long-terminal repeats. *Epigenetics*, 8,
1037 504-11.
- 1038 YAMAGISHI, Y., HONDA, T., TANNO, Y. & WATANABE, Y. 2010. Two histone marks
1039 establish the inner centromere and chromosome bi-orientation. *Science*, 330,
1040 239-43.
- 1041 YANG, W., SOARES, J., GRENINGER, P., EDELMAN, E. J., LIGHTFOOT, H., FORBES, S.,
1042 BINDAL, N., BEARE, D., SMITH, J. A., THOMPSON, I. R., RAMASWAMY, S.,
1043 FUTREAL, P. A., HABER, D. A., STRATTON, M. R., BENES, C., MCDERMOTT, U.
1044 & GARNETT, M. J. 2013. Genomics of Drug Sensitivity in Cancer (GDSC): a
1045 resource for therapeutic biomarker discovery in cancer cells. *Nucleic Acids*
1046 *Res*, 41, D955-61.
- 1047 YOKOYAMA, Y., HIEDA, M., NISHIOKA, Y., MATSUMOTO, A., HIGASHI, S., KIMURA, H.,
1048 YAMAMOTO, H., MORI, M., MATSUURA, S. & MATSUURA, N. 2013. Cancer-
1049 associated upregulation of histone H3 lysine 9 trimethylation promotes cell
1050 motility in vitro and drives tumor formation in vivo. *Cancer Sci*, 104, 889-95.
- 1051 ZHOU, M., LI, Y., LIN, S., CHEN, Y., QIAN, Y., ZHAO, Z. & FAN, H. 2019. H3K9me3,
1052 H3K36me3, and H4K20me3 Expression Correlates with Patient Outcome in

1053 Esophageal Squamous Cell Carcinoma as Epigenetic Markers. *Dig Dis Sci*, 64,
1054 2147-2157.
1055

1056

1057 **Figure Legends**

1058 **Figure 1. High expression of Suv39 and Suv420 isoforms in cancer correlate with**
1059 **aneuploidy and reduced patient survival. A)** Gene expression values for Suv39h1,
1060 Suv39h2, Suv420h1, and Suv420h2 from TCGA, sorted by cancer subtype indicate
1061 increased gene expression compared to normal tissue expression levels in multiple
1062 cancer subtypes. **B)** Suv39 and Suv420 isoform expression exhibit a moderate but
1063 highly significant correlation with calculated aneuploidy score in several cancer
1064 subtypes. Red text indicates significance at $p < 0.0025$. (See also Supplemental Table 1)

1065

1066 **Figure 2. Depletion of KDM4A compromises mitotic fidelity. A)** Still images and
1067 quantification of average mitotic duration from time-lapse microscopy of RFP-H2B
1068 expressing RPE-1 cells transfected with either non-targeting control (siControl) or
1069 KDM4A-targeting (siKDM4A) siRNAs show cells lacking KDM4A exhibit delayed
1070 anaphase onset. Images were captured every 5 minutes. Number insets indicate time
1071 progression in minutes. Nuclear envelope breakdown (NEB) and anaphase onset (AO)
1072 are indicated. 50 mitotic cells were analyzed per condition for each of 3 biological
1073 replicates. **B)** Images and quantification showing KDM4A-depleted mitotic cells have an
1074 increase in late prometaphase/metaphase cells that retain 1-3 unaligned chromosomes.
1075 **C)** Images and quantification showing KDM4A-depleted anaphase cells exhibit an
1076 increase in lagging chromosomes during anaphase. For panels B and C, 30 metaphase
1077 or anaphase cells were analyzed per condition for each of 3 biological replicates. For all
1078 panels, white arrowheads indicate unaligned or lagging chromosomes; *: $p < 0.05$, **: p
1079 < 0.01 . Error bars are +/- SD and statistical analyses were performed between three
1080 biological replicates. Scale bars are 5 μm .

1081

1082 **Figure 3. Increased H4K20me3 corresponds with decreased mitotic fidelity. A)**
1083 Images and quantification showing an increase in lagging chromosomes during
1084 anaphase following induced expression of cen-Suv39-GFP or cen-Suv420-GFP. White
1085 arrowhead indicates a lagging chromosome. Scale bar is 5 μ m. **B)** Images and
1086 quantification showing induction of cen-Suv420-GFP promotes a substantial increase in
1087 centromere-localized H4K20me3 levels, while siKDM4A, cen-Suv39-GFP, and (non-
1088 tethered) Suv420-GFP induce only a moderate changes in H4K20me3 at centromeres.
1089 Cen-GFP does not alter centromere H4K20me3 levels. Insets are 1.5x enlargements of
1090 ACA-stained kinetochore pairs. Scale bar is 1 μ m. **C)** Images and quantification showing
1091 an increase in micronuclei formation following induction of cen-Suv39-GFP or cen-
1092 Suv420-GFP. Insets are 3X enlargements of individual micronuclei. Presence of an
1093 ACA-labeled kinetochore within each micronucleus indicates they likely form following
1094 mitotic segregation errors. Scale bar is 5 μ m. Alignment and segregation errors were
1095 assessed in 30 cells per condition, per replicate. Intensity analyses were done on 10
1096 kinetochores for each of 30 cells per condition, per replicate. For micronuclei analyses, a
1097 minimum of 240 cells were scored per condition, per replicate. All statistical analyses
1098 were performed between three biological replicates, *: $p < 0.05$, **: $p < 0.01$. Error bars
1099 are +/- SD.

1100

1101 **Figure 4. Mitotic error correction and Aurora B localization are compromised when**
1102 **centromere Suv420/H4K20 methylation levels are increased. A)** Images and
1103 quantification showing progression to full metaphase alignment following inhibition of
1104 Eg5 with monastrol and subsequent drug washout. Cells lacking KDM4A or expressing
1105 cen-Suv39-GFP or cen-Suv420-GFP are delayed in achieving metaphase alignment,
1106 indicating a deficiency in mitotic error correction capacity. **B)** Images and quantification

1107 of Aurora B kinase localization at centromeres of nocodazole-treated prometaphase
1108 cells. Induced expression of cen-Suv39-GFP or cen-Suv420-GFP, but not cen-GFP,
1109 reduced Aurora B intensity at centromeres. Insets are 2X enlargements of single ACA-
1110 stained kinetochore pairs. Scale bars are 5 μ m. Kinetochore analyses were done on 10
1111 kinetochores for each of 30 cells per condition, per replicate. Alignment was assessed in
1112 50 cells per condition, per replicate. For all panels statistical analyses were performed
1113 between three biological replicates, *: $p < 0.05$, **: $p < 0.01$. Error bars are +/- SD.

1114

1115 **Figure 5. Inhibition of Suv420 methyltransferase activity restores Aurora B**
1116 **localization and corrects metaphase alignment defects. A & B)** Treatment of cen-
1117 Suv420-GFP expressing cells with 200 nM Suv420 inhibitor A196 reduces H4K20me3
1118 levels and partially restored Aurora B localization to the centromere. **C)** Chromosome
1119 alignment defects seen in cells expressing cen-Suv420-GFP are suppressed following
1120 concurrent treatment with A196. Insets are 2X enlargements of single ACA-stained
1121 kinetochore pairs. Kinetochore analyses were done on 3 kinetochores for each of 30
1122 cells per condition, per replicate. Alignment was assessed in 30 cells per condition, per
1123 replicate. For all panels statistical analyses were performed between three biological
1124 replicates, *: $p < 0.05$, **: $p < 0.01$.

1125

1126 **Figure 6. Increased H4K20me3 reduces phosphorylation of Aurora B target Hec1**
1127 **and increases microtubule stability. A & B)** Images and quantification showing that
1128 pHec1, but not total Hec1 levels at the centromere are decreased following cen-Suv39-
1129 GFP or cen-Suv420-GFP expression. Note that this pHec1 antibody stains both
1130 centrosomes and kinetochores. Insets are 3X enlargements of single ACA-stained
1131 kinetochore pairs. Staining intensity between ACA peaks was measured for 3
1132 kinetochore pairs in each of 30 metaphase cells per condition, in each of 3 biological

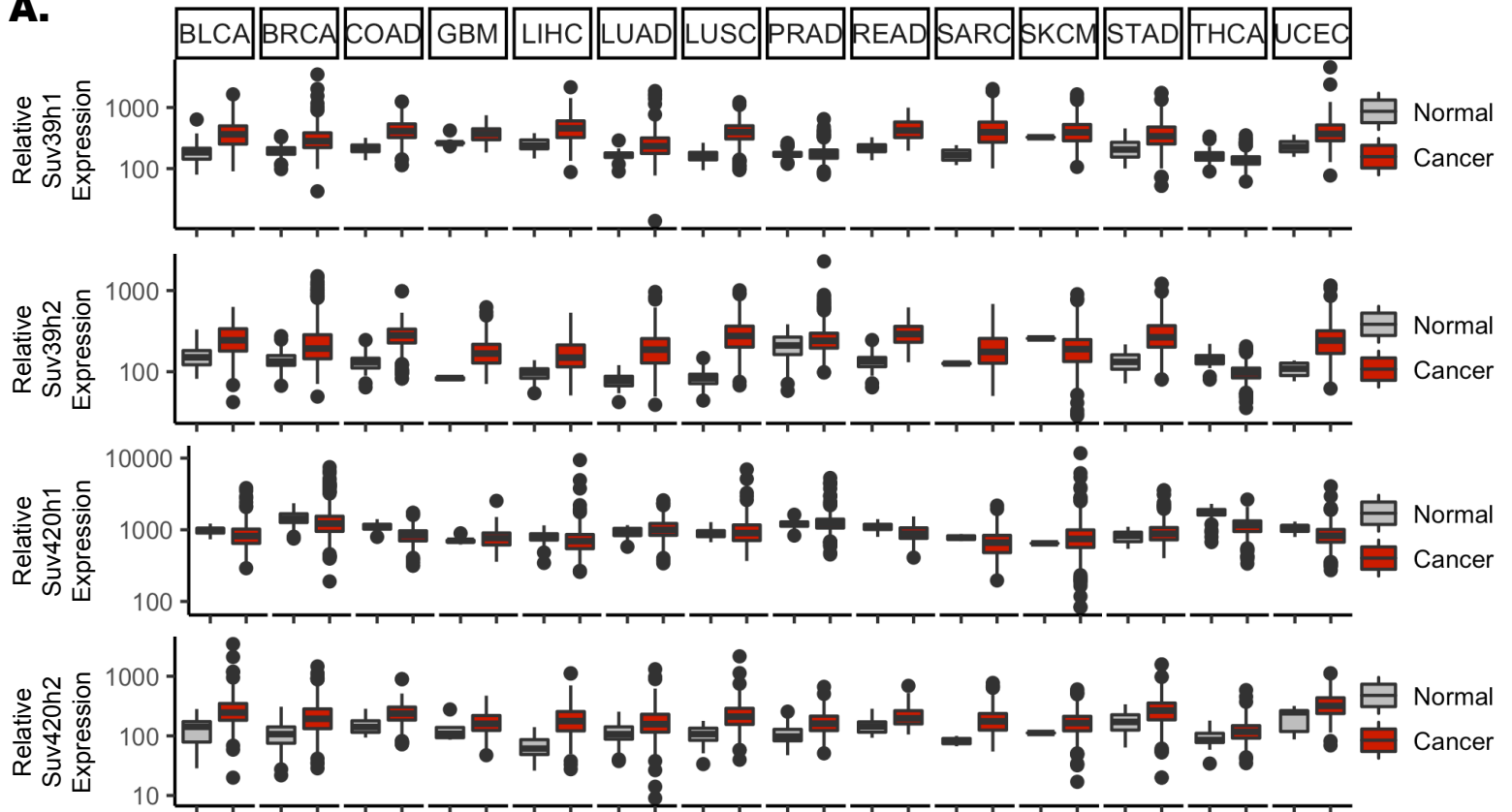
1133 replicates. **C)** Images and quantification showing that induction of cen-Suv39-GFP or
1134 cen-Suv420-GFP expression increases the resistance of kinetochore microtubules to
1135 cold-induced depolymerization, indicating an increase in stability of kinetochore-
1136 microtubule attachments. Microtubule intensity was measured in each of 30 metaphase
1137 cells per condition, in each of 3 biological replicates. *: $p < 0.05$, **: $p < 0.01$. Scale bars
1138 are 5 μm .

1139

1140 **Figure 7. Expression of Suv39 and Suv420 sensitizes cells to Aurora kinase**
1141 **inhibition. A)** Quantification of anaphase defects showing that cells induced to express
1142 cen-Suv39 or cen-Suv420 exhibit an increase in anaphase lagging chromosomes
1143 following low nanomolar concentrations of Aurora kinase inhibition while their uninduced
1144 counterparts do not. Cells both with and without induction of cen-Suv39-GFP or cen-
1145 Suv420-GFP are similarly sensitive to inhibition of the mitotic kinase MPS1. (+/- cen-
1146 Suv39-GFP induction: $p = 0.00003$, 0.0003 , and 0.844 for Alisertib, Barasertib, and
1147 MPS1IN1, respectively; +/-cen-Suv420-GFP: $p = 0.003$, 0.004 , and 0.724 for Alisertib,
1148 Barasertib, and MPS1IN1, respectively) Error bars are +/- SD. **B & C)** Cen-INCENP-
1149 mCherry localizes to centromeres in cen-Suv420-GFP expressing cells. **D)** Expression
1150 of cen-INCENP-mCherry does not limit cen-Suv420-GFP localization to centromeres.
1151 GFP-staining intensity between ACA peaks was measured for 3 kinetochore pairs in
1152 each of 30 metaphase cells per condition, in each of 3 biological replicates. **E)**
1153 expression of cen-INCENP-mCherry reduces the frequency of lagging chromosomes
1154 seen in cen-Suv420-GFP expressing anaphase cells. A minimum of 30 anaphase cells
1155 were scored per condition, for each of 3 biological replicates. **: $p < 0.01$, ***: $p < 0.001$.
1156 **F)** Quantification of area under the dose response curve (AUC) for each drug in cancer
1157 cell lines from the TCGA sorted by top and bottom quartile of either Suv39 or Suv420
1158 expression shows that cells with high expression of either Suv39 or Suv420 exhibit

1159 increased sensitivity to Aurora kinase inhibition. Each dot represents an individual
1160 cancer cell line tested. Open circles indicate the mean of IC50 AUCs for each condition.
1161 *: $p < 0.00625$, **: $p < 0.00125$, ***: $p < 0.000125$. Error bars are +/- SEM.

A.



B.

